EasyChair Preprint

№ 8507

Design and Analysis of Compact Microstrip Patch Antenna for LTE Applications Using Metamaterials with Artificial Intelligence in Special Use.

Shubham Singh and Jaswant Kumar

July 20, 2022

DESIGN AND ANALYSIS OF COMPACT MICROSTRIP PATCH ANTENNA FOR LTE APPLICATIONS USING METAMATERIALS WITH ARTIFICIAL INTELLIGENCE IN SPECIAL USE .

Shubham Singh
M.Tech [E.C.E] Scholar
Electronics & Comm. Engg.
ABSSIT, Meerut
shubhamtitm@gmail.com

Mr. Jaswant Kumar
Lecturer
Dept. of Electrical Engineering
Govt. Polytechnic Chhachha, Mainpuri
jaswant.knit2011@gmail.com

1. Abstract :

The work presented in this thesis channel through the development of novel microwave structures and techniques for realizing compact planar antennas for LTE-band operation. The preliminary antenna designs were investigated by modelling microwave patch antenna and loading metamaterial complementary split ring structures. The single and dual-band resonant of the antenna confirm the advantage of the metamaterial-based antenna for multi-band operation and compact. Subsequently, defective grounding technique was analysed and modeled in the antenna design for obtaining a narrow and selective frequency band.

Further, the design of a miniaturized dual-band planar antenna for LTE application and the generation of narrow triple bands using the stacking concept of dielectric resonator and metamaterial unit-cell were developed. In the basic antenna design, split ring resonator was loaded in the radiating plane of the patch and frequency of resonance was further modified with the help of E-shaped stub. The antenna has been fabricated using FR-4 substrate and the measured dual bands at 2.11 GHz, and 2.665 GHz are found in a close match with the simulated data. By placing a thin dielectric resonator of permittivity ε_r =10.2 and thickness of 1.27 mm, the separation between the bands is reduced, and two closely spaced narrow bands are obtained at 2.217 GHz and 2.28 GHz. A novel metamaterial unit-cell having near-zero refractive index is designed and mounted above thedielectric resonator. This stack configuration generates triple narrow frequency band in the LTE 2 GHz spectrum range. The overall size of the proposed antenna is 20 × 25 mm^2 and found suitable for narrowband communication in the LTE spectrum.

In the final stage, a compact antenna design with wide spectral frequency diversity in a wireless system was implemented. Planar antenna using

defective ground and coarse frequency switching with connected split-ring resonator through PIN diodes are presented. The antenna design is based on connected radial stubs which form a patch. Slots in the bottom plane create a corrugation-like structure. This results in the defective ground, whichcontributes to the localization of electric flux at the different areas in the antenna plane for multiband operation. The antenna was simulated and fabricated on a 1.6 mm thick FR-4 substrate. The coarse tuning of the frequency band is tested and compared with the simulation data. The measured results depict broadside radiation pattern at different frequency bands (like 0.96 GHz, 2.63 GHz, 3.22 GHz) and with a peak gain of 3.72 dBi. The compact size (45 × 45 mm^2) and diversity frequency resonance up to pentaband in the antenna makes it suitable for LTE and WLAN/WiMAX application systems. From the proposed antenna designing techniques and their practical implementation, it is observed that modifying the antenna topology using metamaterial, dielectric resonator, defect ground and metering stubs is proven as a goal-oriented approach for planar LTE band microstrip antennas.

Introduction :

The planar antenna has always been a necessary element in the evolution of sophisticated wireless communication systems, and it provides an effective means for free- space communication through electromagnetic waves. Recent advancements in the wireless standards have increased the demand for multiband antennas that can operate on multiple frequencies with desired bandwidth . The need for higher bandwidth or multiple narrowband resonances in the antenna carter essential functions such as spectrum sensing, smart allocation of data on multiple frequency channels and selective communication for various applications related to the industrial, defence, and biomedical.

Keywords: single-feed; circularly polarized microstrip patch antenna; periodic structure

2. Antenna design

A circular microstrip patch antenna and with a circularly periodic EBG structure was designed using CST Microwave Studio software. The EBG structure and the three layers, including the air layer, were designed to increase the gain of the patch antenna at its operating frequency, which was arbitrarily selected to be 3.08GHz. Fig. 1 shows a conventional CPA for comparison with the antennas developed in this study. The radius of the patch was 17.5mm, its thickness was 0.508mm, and the permittivity of the substrate was 2.5 at 3.08GHz. The patch was fed by a coaxial

line 5mm from its center. The return loss and gain of this antenna are shown in Fig. 2. The feed location was optimized to provide good impedance matching. The substrate dimensions were 180 × 180 mm. The maximum gain of the patch antenna was approximately 5dB, and the input impedance bandwidth was about 22.6MHz, or 0.7% of the 3.08GHz operating frequency. Fig. 3 shows the antenna configuration with an air substrate between two dielectric substrates; each dielectric substrate is the same as that shown in Fig. 1. The dielectric constants and thicknesses of the first and third substrates were 2.5 and hd . Based on a three-layered cavity model.

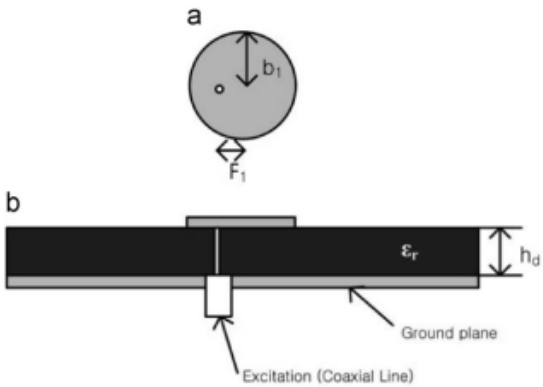

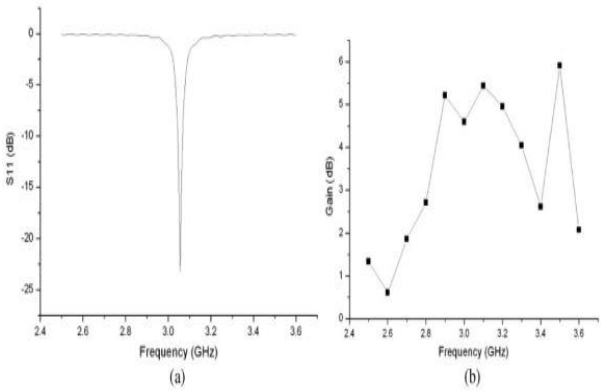

Fig. 2. CPA (a) simulated return loss and (b) gain.

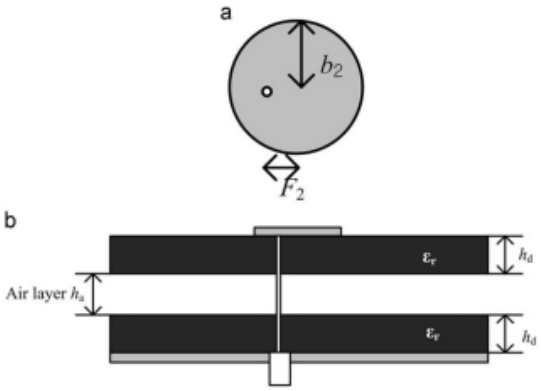

Fig. 3. Detailed geometry of the ($CPA_{Air\ layer}$): (a) top view and (b) side view.

analysis [2], a simple and more general expression for the resonant frequency of TM_{nm} modes of a circular patch antenna with an air layer can be given as

$$f_{nm} = \frac{\omega_{nm}}{2\pi} = \frac{\chi_{nm}}{2\pi b\sqrt{\mu_0 \varepsilon_{eff}}} \qquad (1)$$

3. Model Validation:

The validity of the modal approach for the design of a patch antenna with an EBG surface underneath is further investigated through a full-wave 3-D numerical simulation of an EBG loaded

patch antenna. The EBG parameters used are: UC 10 mm 10 mm, EBG patch 8.5 mm 8.5 mm, vias radius 0.2 mm, substrate thickness 1.5748 mm (EBG surface in the middle), and all dielectric layers are FR-4 materials. Conventional rectangular microstrip patch antennas operate at the fundamental TM mode. As was discussed in Section II, this also seems to be the case for a patch antenna over an EBG substrate, except with a reduced wavelength as observed in the dispersion diagram. In this section, the resonant frequency of a rectangular patch antenna on top of an EBG (mushroom) structure is investigated through the use of the Zeland IE3D full-wave solver (moment method code). An open-circuit microstrip line at the EBG surface is proximity-coupled to the radiating patch. Resonant frequencies for a set of square radiation patch lengths (10, 20, 30, 40, 50, and 60 mm) are found from the return loss dip under a frequency sweep. Since the fundamental patch resonant frequency depends mostly on the propagation wavelength of the substrate, the corresponding linear dimension of patch antenna is close to half-wavelength. Both the UC and FCS-EM analyses are used to produce the antenna resonant length based on a half-wavelength approximation. The results are shown in Fig. 3. The FCS-EM analysis is found in very good agreement with the 3-D antenna simulation. It confirms the validity of the half-wavelength transmission line approach and the accuracy of the modal analysis. A discrepancy is observed for the UC-EM analysis when the patch width becomes narrow compared to an EBG UC length.

As an example, for a patch size of 10 mm 10 mm, both full-wave 3-D simulation and FCS-EM modal analysis show that the patch resonant frequency is about 2.92 GHz (way into the parallel-plate bandgap zone), while the UC model shows that the EBG patch antenna frequency is 2.41 GHz (for a wavelength of 20 mm). This discrepancy implies that the UC parallel-plate As an example, for a patch size of 10 mm 10 mm, both full-wave 3-D simulation and FCS-EM modal analysis show that the patch resonant frequency is about 2.92 GHz (way into the parallel-plate bandgap zone), while the UC model shows that the EBG patch antenna frequency is 2.41 GHz (for a wavelength of 20 mm). This discrepancy implies that the UC parallel-plate .

TABLE I
RESONANT FREQUENCIES OF A SQUARE PATCH ANTENNA

Patch Dimension (mm^2)	Plain Antenna Resonant Freq [GHz]	EBG Antenna Resonant Freq [GHz]
10x10	6.29	2.92
20x20	3.32	2.15
30x30	2.25	1.67
40x40	1.71	1.27
50x50	1.38	1.03
60x60	1.15	0.85

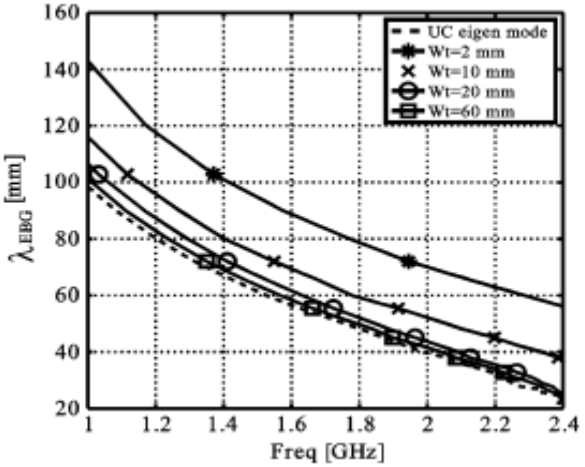

case of a patch), its width and the location of the strip relative to the EBG surface profiles are insignificant to the phase constant (patch antenna length) and the UC-EM cavity model works well even with an EBG surface insertion. It is observed from Fig. 4 that the FCS-EM modal analysis can also be used to design a half-wavelength thin dipole antenna above an EBG surface.

Prototype Of A Patch Antenna Above An Ebg Surface

A prototype of linear-polarized microstrip antenna on a mushroom-like EBG substrate is fabricated and tested. Antenna return loss and radiation pattern are investigated and compared to those of a conventional microstrip patch antenna. The configuration of a microstrip antenna with an EBG substrate is depicted in Fig. 8. The antenna structure includes two 0.7874-mm-thick (31 mil), 70-mm-long, and 85-mm-wide dielectric FR4-epoxy layers, with parameters and loss tangent 0.01. The EBG patch arrays with 6 8 mushroom-like UCs are in the middle of the cavity. The rectangle radiation patch is etched above the top FR4 substrate, with dimension 22.14 mm and 31.59 mm. The EBG UC size is 7 mm, EBG patch dimension is 4.5 mm 4.5 mm, and grounding vias radius 0.2 mm. Dispersion diagram obtained from the modal analysis is already shown in Fig. 2. It predicts that the wavelength is about 42 mm (21 mm) at 2.5 GHz and serves as the initial design. All the EBG planar texture and vertical vias are designed and fabricated in the bottom FR4 substrate. In addition, a 50 open-circuited microstrip line (1.2 mm in width) is also printed on the same surface as the EBG patches, and proximity-coupled to the upper radiation patch. Two dielectric substrate layers are finally laminated together by multilayer PCB technique to form a low-profile planar antenna. The 3-D full-wave IE3D simulation is used to fine-tune the patch length. The simulated and measured results of the

return loss are given in Fig. 9. A conventional microstrip antenna with the same size radiation patch is also designed and tested as a reference. The simulation predicts the resonant frequency at 3 GHz, while the measurement shows the resonance at 3.18 GHz, for a normal patch antenna. In contrast, the resonant frequency of an EBG patch antenna is predicted at 2.48 GHz by 3-D full-wave IE3D simulations (with 2 2.14 mm) and at 2.52 GHz by measurement. Both the simulation and measurement results show that after introducing EBG patterns in the bottom dielectric substrate, the resonant frequency of patch antenna and the bandwidth both decrease. The discrepancies between simulations and measurements are basically due to the tolerance of PCB fabrication. The decrease in resonant frequency for an EBG antenna is due to the capacitive and inductive loadings of the EBG profiles under the patch. The decrease in bandwidth is probably due to fact that the ground backing of the patch antenna is effectively moved up to the EBG surface and reduces the effective substrate thickness, and the patch antenna bandwidth is roughly proportional to the substrate thickness. The radiation patterns of an EBG patch antenna are measured in an anechoic chamber room at 2.5 GHz. Both simulated and measured - and -plane patterns are shown in Figs. 10 and 11, respectively. The main beam direction at the first resonant frequency 2.5 GHz is in broadside direction normal to antenna surface, and the corresponding antenna gain is about 3.75 dBi. The backward radiation of EBG patch antenna is at around 15 dBi, which is at about the same level of a conventional patch antenna. In general, comparison between simulation and measurement shows very good agreement. The radiation patterns for an EBG patch are similar to those of a normal microstrip patch antenna at its fundamental mode.

4. Antenna Geometry

The geometry of the proposed antenna. It is composed of two layers with an air-gap in between. A probe-fed circular patch with two separated circular slots as a driven patch that placed below a stacked layer at distance of hair is investigated. The driven patch is designed to have a resonant frequency of 2.45 GHz, which its dimensions were modified from the design presented in Ref. 12. In this case, the antenna was designed to realize left-hand circular polarization (LHCP). It is etched on an inexpensive FR4 substrate with dielectric constant of 4.2. A stacked layer consists of 4 4 square rings joined with diagonal-strips (SQRDS). Usually, the conventional.

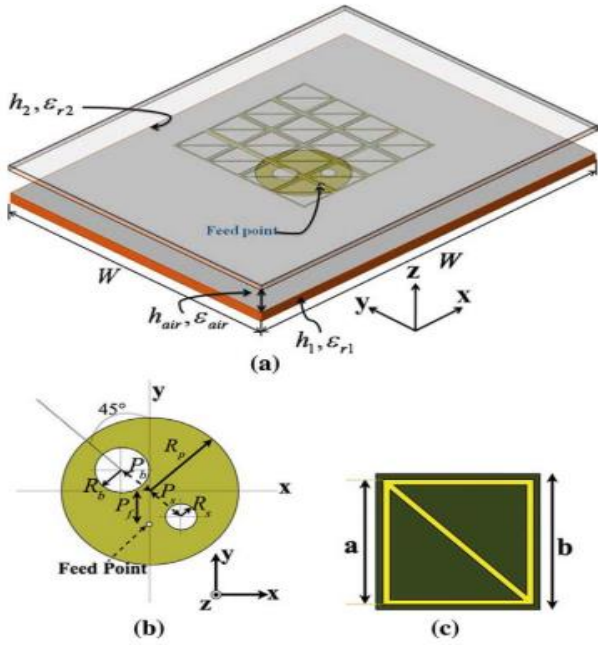

Figure 1 (a) configuration of the proposed antenna, (b) unit cell SPS, and (c) driven CP-MPA. Geometry parameters are (unit: mm): a 18, b = 20, R_p = 15.6, R_b = 5.4, R_s = 2.4, P_b = 5.4, P_s = 8.4, P_f =1 h_1 = 1.6, h_2 = 0.8, h_{air} = 7.5, and $\varepsilon_{r1} = \varepsilon_{r2}$ = 4.2. [Color figure can viewed in the online issue, which is available at wileyonlinelibrary.con

5. Antenna Analysis And Parametric Study

In previous sections, the performance of the CP-MPA with SPS is presented. To accurately design the proposed antenna for practical applications, its operating principles should be studied carefully. The performance of the proposed antenna structure shows greater sensitively to variation in some parameters including the height of air gap (hair) and array size of SPS.

First of all, the height (hair) between the driven patch and stacked layer is very stringent to produce good CP waves for the stacked configuration. Since the distance between source patch and the SPS is small (k/10), the coupling mechanism exists, this configuration is categorized as electromagnetically coupled technique [13]. The variation of return losses, ARs and realized gains are shown in Figure 6. As hair increases from 6.5 to 9.0 mm, impedance bandwidth becomes narrow with poor matching. From the results as shown in Figure 6(a), the height of air gap mainly affects the frequency corresponding to the lower edge of the bandwidth, whereas it has minimal effect on the frequency corresponding to the upper edge. With increase in the hair, the total height of the antenna increases, and the effective dielectric constant (eeff) by the SPS reduces its resonant frequency. It is also observed that the hair has a significant effect on AR bandwidth as observed from Figure 6(b). As hair is 8.5 and 9.0 mm, a V-shaped curve of AR is obtained. For hair ¼ 7.5 and 8.0 mm, the AR is below the 3-dB yielding a bandwidth of 230 and 200 MHz (10 and 9%), respectively. This antenna covers the frequency band of 2.40–2.48 GHz of the WLAN. When hair ¼ 7.5 mm, a W-shaped curve of AR is obtained which guarantees the maximization of the 3-dB AR bandwidth. We achieve the best simulated result when hair is 7.5 mm. Therefore, this parameter can be used to choose AR bandwidth. It is also found that the realized gains are hardly affected by the height of air gap as shown in Figure 6(c). By increasing hair further, the gain of the antenna can be increased from 7.2 to 8.5 dBi in operating.

6. Evolution of LTE Communication Technology

The Long-Term Evolution (LTE) technology is a huge step in communication technology. The continuous expansion of LTE into the upcoming systems is due to the growing demand for high-speed packet and need

for large channel capacity. The evolution of LTE is illustrated in Fig. 1.1 [1]. The advancement in wireless communication technology can be categorized into different generations in which each preceding generation has overcome the limitations of the previous. The first generation (1G) mobile communication devices consisted of analog systems. The 1G technology supported voice- only services and no roaming. This technology featured frequency modulation (FM), frequency division duplexing (FDD), and Frequency division multiple access (FDMA) methods. Mainly monopole type antennas were used for single-band communication. First- generation wireless systems were having several limitations such as low capacity, inconsistent voice quality, cross-talk between users, and bulky equipment [3].The 2G systems were mainly dependent on digital signal modulation to provide a much higher bandwidth capacity as well as digital encryption [4]. The combination of consistent voice quality along with relatively small-sized devices attracted a wide variety of applications. Time-division multiple access methods (TDMA) was one of the prominent channel access methods in the 2G wireless systems. GSM (Global System for Mobile) and PDC (Personal Digital Cellular) were some of the 2G standards based on this time-divisionmethod

7. LTE Frequency Bands

LTE technology offers not only higher performance but also reduced capital and operating costs. The primary goal of LTE was to evolve within the existing infrastructure. Thus, several existing frequency bands of different wireless standards were adopted for the allocation of the LTE frequency band. The LTE spectrum can be split into two main categories based on the duplexing methods i.e ., Frequency Division Duplexing (FDD) and Time Division Duplexing (TDD). In Table 1.1 and Table 1.2, the allocation of uplink and downlink frequency bands are mentioned.

TABLE 1.1 Details of frequency bands of FDD LTE [4]

Band Number	Uplink (MHz)	Downlink (MHz)	Main Regions
1	1920 -1980	2110-2170	All
2	1850-1910	1930-1990	NA
3	1710-1785	1805-1880	All
4	1710-1755	2110-2155	NA
5	824-849	869-894	NA
6	830-840	875-885	APAC
7	2500-2570	2620-2690	EMEA
8	880-915	925-960	All
9	1749.9-1784.9	1844.9-1879.9	APAC
10	1710-1770	2110-2170	NA
11	1427.9-1447.9	1475.9-1495.9	Japan
12	699-716	729-746	NA

2.1.1 Frequency Reconfigurable Antenna

Frequency reconfigurability allows many different antenna design implementations using stubs, slots, and resonators. By using active elements like PIN diode or varactor diode, coarse tuning or fine-tuning of frequency bands is achieved. The PIN diode connects part of the antenna to either a resonator or a metering stub. This changes the total electrical length of the antenna and proper frequency diversity is obtained. On the other hand, by using varactor diode, the reverse junction capacitance of the diode contributes toa minor or major change in electrical length of the antenna depending upon its position with respect to the feed point S. Danesh et al . [48], reported a compact frequency - reconfigurable antenna using four resonators, each loaded with a dielectric material and PIN diode was connected between the two elements. The antenna schematic is shown in Fig. 2.13. The total dimension of the antenna is 20×36 mm^2 and fabricated using a low-loss material substrate (Taconic) of relative permittivity 3.2. The dielectric resonators of dielectric constant 10 excited.

The different switching conditions of the PIN didoes results in four different resonant frequencies at 1.89 GHz , 2.14 GHz, 2.53 GHz, and 2.77 GHz , as shown in Fig . 2.14. Also,the partial ground plane helps in obtaining an eight-shaped radiation pattern, which is broadside in nature. Such techniques are useful for designing a compact and performance oriented antenna for various LTE band applications.

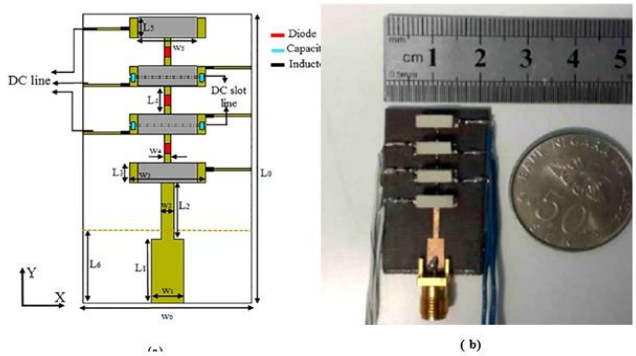

FIGURE 2.13 (a) Schematic of the reconfigurable antenna with dielectric resonators, (b) Image of the fabricated prototype antenna [48].

2.2 Research Gap and Motivation

The antennas for fourth generation (4G) long-term evolution (LTE) are under continuous development for achieving a compact design with multiple frequency bands. Inrecent years, a high data rate in LTE technology has attracted many personal wireless applications for industrial and scientific areas, especially in the LTE-A band (2 GHz) [52]. To support the channel capacity in the operating frequencies of LTE system, electrically small antennas are needed in the customer premises equipment (CPE) and handheld receivers. To meet the emerging requirements of LTE communication, various microwave techniques, along with multiple-input multiple-output (MIMO) mode are

reported. I. Dioum et al. [53], introduced a novel compact design of 3D inverted-F-antenna (IFA) with MIMO for dual-band of LTE 700 and LTE 2.5-2.7 GHz. Generally, single resonance is obtained in such designs, and more than one frequency band is generated with the help of parasitic elements [54]. The design of the MIMO antenna with a shaped dielectric resonator (DR) solves the problem of achieving a low-frequency band of LTE band 12 and 17 [55]. In such a design, a coaxial probe and microstrip line are employed simultaneously and placed in the close vicinity of the DR [56-58]. In addition to this, different shapes like C-shape [59], F-shape [60], sectored conical [61] and tetraskelion [62] are either coupled

with the feed line or placed above the slotted patch for wideband applications. Recently, dual-band antennas integrated into the last stage of the filter are being proposed for LTE systems [63, 64]. However, in these filtering antennas, the insertion loss is higher due tothe presence of the filter circuit. X. Y. Zhang [45] developed a dual-band filtering patchfor MIMO LTE in which two U-shaped slots were incorporated into the patch and a multi stub feed line was used to excite resonant modes for B39- and B38-band. Another concept of providing a separate single path to a ring resonator is reported by Y. Zhang [65], wherein good isolation between the antennas is achieved. D. Sarkar and coauthor presented a split ring resonator (SRR) loaded four inverted L-monopole printed antennas having 4G LTE band (3.4-3.6 GHz) with an omnidirectional radiation pattern and isolation (> 14 dB) amongst the radiators [47]. Besides the MIMO configurations, LTE tablet computer antenna and smartphone antenna in PIFA technology are widely utilized. The antenna developed by K. –L. Wong and co-authors explore various designs of the LTE antenna [66-68]. These involve coupled fed stripline antenna with inductive coupling through microstrip and lumped elements, two antennas mounted on the edge of the metal plate, and dual feed U-shaped open slot antenna at the top and bottom side of the ground plane. The microwave technique comprising of the stacked dielectric resonator of different permittivity is found to improve the quality factor (Q) of the antenna, which contributes to the narrowband resonance. A. K Jyani [69] realized such an antenna using a coaxial probe and two or more DR‟s.

Conclusion :

In this work, the rectangular microstrip patch antenna is designed using the artificial neural network modeling procedure. Here synthesis refers to forward side and analysis refers to reverse side of the problem. Therefore in synthesis problem, the geometric dimensions such as length and the width of antenna are obtained with more accuracy in less time as compared to simulation software while providing resonant frequency, thickness, and dielectric constant at the input side of the ANN model. In the analysis problem of patch antenna, resonant frequency or both upper and lower cutoff frequencies of patch antenna are obtained at the output side of the ANN model while providing the dimensions of patch (W, L) and other parameters at the input side of the ANN model with much accuracy in less time. Now the future work in this work includes trying more topologies to obtain more compact patch antennas, filters, and many other microwave/RF modeling design using artificial neural network for different band of applications such as ultra-wideband (UWB), Global System for Mobile communications (GSM), and WiMAX applications.

The gain of a CPA was improved using an EBG structure with an air layer. The antenna was composed of a periodic structure of circular metallic rings around the circular microstrip patch in the upper layer, an air layer in the middle, and a dielectric substrate on the bottom ground layer. The parameters of the EBG structure (spacing, width of the EBG elements, and number of EBG elements) and the thickness of the air layer were optimized using CST Microwave Studio to obtain the maximum gain. While the EBG structure reduced the surface wave, the gain enhancement was due mainly to the coupling between the patch and the EBG structure. The air layer in the middle provided a substrate with a lower effective permittivity and increased thickness for the higher gain antenna. The experimental results showed that the gain of CPAEBG Air layer was 11.9dB, an improvement of 6.5dB over that of the CPA

References:

[1] C. Cox, Introduction to Mobile Telecommunications, Cambridgge University Press, 2012.

[2] C. S. Patil, R. R. Karhe and M. A. Aher, "Review on Generations in Mobile Cellular Technology," International Journal of Emerging Technology and Advancement in Engineering, vol. 2, no. pp. 614-619, 2012.

[3] M. R. Bhalla and A. V. Bhalla, "Generations of mobile wireless technology: A survey," International Journal of Computer Applications, vol. 4, no. 4, pp. 26-32, 2010.

[4] E. Dahlman, S. Parkvall and J. Skold, 4G LTE/LTE-Advanced for Mobile Broadband, Elseiver Academic Press, Amsterdam, 2011.

[5] ITU-R, "Principles for the process and developnent of IMT-Advanced," Resolution ITU-R 57, pp. Oct. 2007.

[6] D. Gesbert and J. Akhtar, "Breaking the barriers of Shannons Capacity: An overview of MIMO wireless systems," Signal Prcessing, vol. 1, no. B2, pp. B3, 2002.

[7] D. M. Pozar, Microwave Engineering, Wiley, New York, USA, 2005.

[8] R. N. Simons, Coplanar Waveguide Circuits, Components, and Systems, Wiley, New York, 2001.

[9] C. A. Balanis, Antenna Theory: Analysis and Desing, John Wiley & Sons, New Jersey,20005.

[10] R. Garg, P. Bhartia, I. Bhal and A. Ittipiboon, Microstrip antenna design handbook. Boston: Artech House, 2001.

[11] J. S. Hong and M. J. Lancaster, Microstrio Filters for RF/microwave Applications, John Wiley & Sons, New York, 2001.

[12] K. Chang, I. Bhal and V. Nair, RF and Microwave Circuit and Component Design for Wireless Systems, John Wiley & Sons, 2002.

[13] V. G. Veselago, "The Electrodynamics of Substances with Simultaneously Negative Values of Permittivity and Permeability," Soviet Physics Uspekhi, vol. 10, no. 4, pp. 509-514, 1968.

[14] J. B. Pendry, A. J. Holden, D. J. Robbins and W. J. Stewart, "Magnetism from conductors and enhanced nonlinear phenomena," IEEE Transactions on Microwave Theory and Techniques, vol. 47, no. 11, pp. 2075-2084, 1999.

[15] D. R. Smith, W. J. Padilla, D. C. Vier, S. C. Nemat-Nasser and S. Schultz, "Composite Medium with Simultaneously Negative Permeability and Permittivity," Physical Review Letters, vol. 84, no. 18, pp. 4184-4187, 2000.